ACS OMEGA

Article

Cite This: ACS Omega 2020, 5, 358−368

http://pubs.acs.org/journal/acsodf

Preparation of Lignin Nanoparticles with Entrapped Essential Oil as a Bio-Based Biocide Delivery System

Florian Zikeli,*,† Vittorio Vinciguerra,† Simona Sennato,‡ Giuseppe Scarascia Mugnozza,*,† and Manuela Romagnoli*,†

†Department for Innovation in Biological Systems, Food and Forestry, University of Tuscia, Via S. Camillo de Lellis, snc, 01100 Viterbo, Italy

‡Istituto dei Sistemi Complessi, CNR-INFM SOFT and Universitá di Roma "La Sapienza" Roma, Piazzale Aldo Moro, 2, 00185 Roma, Italy

ABSTRACT: Lignin isolated from beech sawdust was used for the preparation of lignin nanoparticles (LNPs) with entrapped essential oil (EO) from cinnamon bark (*Cinnamomum zeylanicum* Blume), common thyme (*Thymus vulgaris* L.), and wild thyme (*Thymus serpyllum* L.) using a fast antisolvent method. Analysis of EO-loaded LNPs by pyrolysis-gas chromatography−mass spectrometry and Fourier transform infrared spectroscopy confirmed molecular interaction between EOs and LNPs. Quantification of EO incorporation into the LNPs and their in vitro release profiles were assessed by reversed phase high-performance liquid chromatography. Utilized EOs were, to different extents, successfully entrapped inside LNPs, which were attributed to extensive π-stacking between aromatic compounds in EOs like cinnamaldehyde, thymol, and carvacrol on one side and aromatic lignin units on the other side. In vitro release of common thyme and wild thyme EOs from EO-loaded LNPs was strongly delayed compared to the use of pure oil, giving a promising outlook for the development of new bio-based biocide delivery systems for wood preservation.

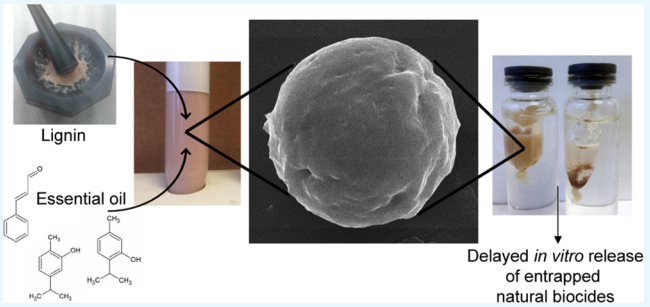

INTRODUCTION

Since mankind has started using wood for their own needs, the problem of its degradation has emerged limiting its use in specific outdoor environments,[1] that is, in the use classes 3 to 5 according to EN 335:2013,[2] where wood deterioration by fungi, bacteria, and insects causes significant economic and resource loss.[3,4] Thus, extending the service life of wood and wood products has always been of huge interest and different strategies against wood degradation have been elaborated. Selection of naturally durable and actually underexploited wood species could establish new wood resources for future technological applications.[5−7] Further, physical treatments, that is, heat treatments, rendering wood less susceptible to decay were applied successfully.[8,9] Traditional chemical treatment agents for wood durability improvement, for example, chromated copper arsenate, creosote, pentachlorophenol, and inorganic arsenicals, have been utilized until today, eventually causing environmental problems as well as affecting human health.[5,10−12] Consequently, over time, environmentally friendly solutions able to reduce or eliminate the use of classic wood preservatives were demanded due to toxicity concerns.[13] In the past decade, interest has gradually focused on naturally occurring compounds and in particular essential oils (EOs) showed promising results regarding prevention of wood decay. Their activity against pathogenic microorganisms was tested in several works, and compounds as thymol, cinnamaldehyde, eugenol, and carvacrol were identified as effective biocides against wood-decaying bacteria as well as against white-rot and brown-rot fungi.[13−17] However, certain limitations for the utilization of EOs in wood preservative formulations exist, that is, regarding their retention inside the wood matrix or their stability toward bio- and photodegradation, as reviewed in detail by Singh T. and Singh A. P.[17]

Introduction of nanoparticles (NPs) in the development of future wood preservatives enables utilization of biocides at low concentrations as well as a controlled release of the entrapped biocide. Indeed, due to their small size, NPs can successively overcome limitations by a wood structure when smaller than window pits (10 nm) and membrane openings in bordered pits (400−600 nm) in softwood or than vessels (<50 μm) in hardwoods. Through encapsulation or entrapment biocides in NPs gain prolonged activity, a lower and controlled leaching rate and a shielding against UV-induced wood degradation extend the service time of treated wood and wood products.[18] Due to their aromatic structure, LNPs are considered a promising carrier for biocides providing substantial protection against sunlight-induced degradation processes and oxidation

Received: August 29, 2019
Accepted: December 2, 2019
Published: December 30, 2019

DOI: 10.1021/acsomega.9b02793
ACS Omega 2020, 5, 358−368

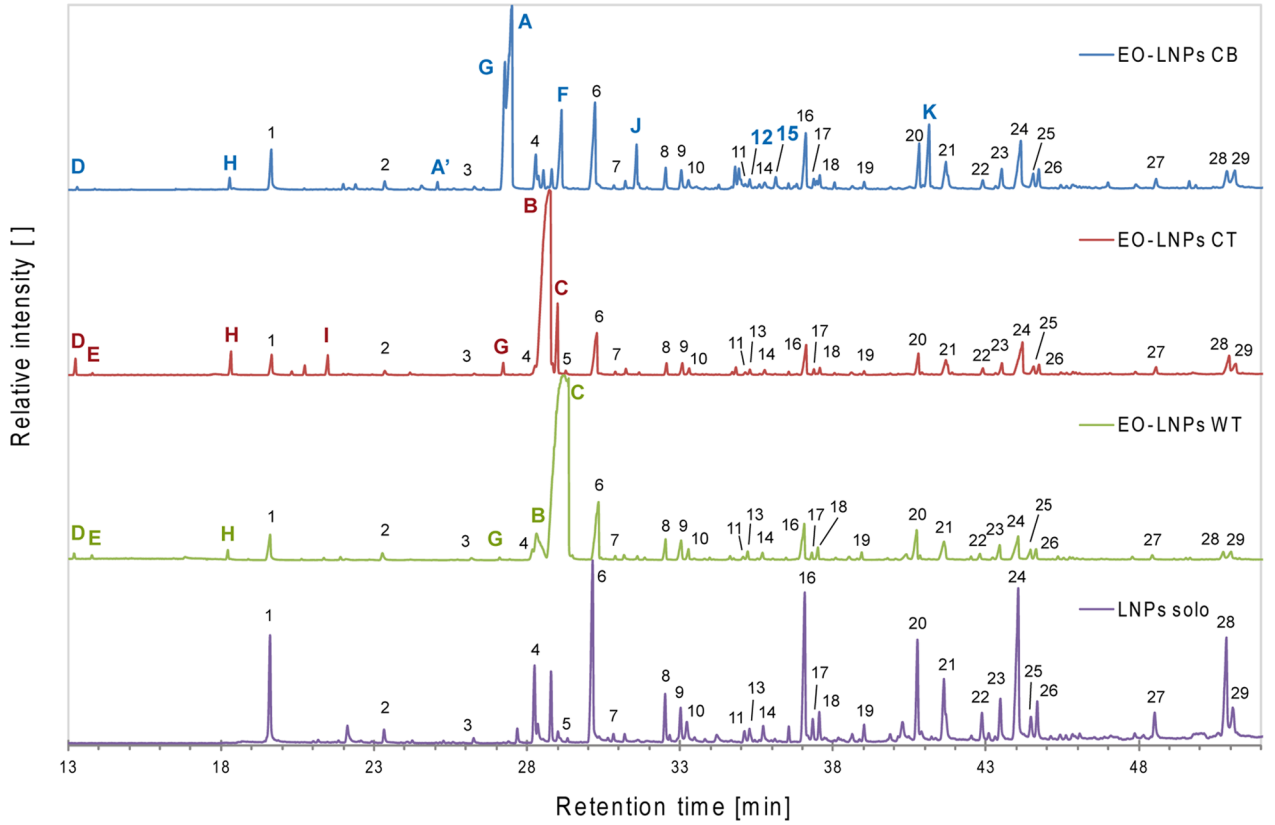

Figure 1. Pyrolysis-GCMS runs of pure lignin nanoparticles (LNPs solo) and LNPs loaded with essential oil from cinnamon bark (EO-LNPs CB), common thyme (EO-LNPs CT), and wild thyme (EO-LNPs WT). Lignin pyrolysis products corresponding to the peak numbers are given in Table 1, bold letters represent components of the respective EOs illustrated in Figure 7, and bold colored numbers represent pyrolysis products deriving from EO components.

increasing stability of biocides.[19] Lignin's natural chemical heterogeneity, as shown, that is, for chestnut lignin from different Italian regions by pyrolysis-GCMS,[20] might be an obstacle for its use as a carrier matrix in biocide delivery systems (BDSs). However, several literature reports in the past years prove the compatibility of lignin as a matrix for controlled release of biocides or drugs, as recently reviewed in detail.[21,22]

In our recent work, LNPs were prepared via an environment-friendly dialysis method using DMSO as a lignin solvent and successively applied on wood surfaces where LNPs showed a tendency to create film-like structures on the woody substrate under UV radiation.[23] With the vision of active lignin coatings for wood protection applications, this work's aim was to prepare and test a novel BDS consisting of LNPs and entrapped essential oils from cinnamon bark (*Cinnamomum zeylanicum* Blume), common thyme (*Thymus vulgaris* L.), and wild thyme (*Thymus serpyllum* L.). Release behavior of the entrapped essential oils was studied by a dialysis method in water, designed as an extreme case of wet outdoor conditions where novel active lignin coatings could be applied.

RESULTS AND DISCUSSION

Qualitative Analysis of the Loaded EO-LNPs by Py-GCMS. Py-GCMS of the prepared freeze-dried EO-LNPs was applied to obtain a complete picture of their components when analyzing the whole sample at once: in the respective pyrograms, beside the common lignin pyrolysis products, also the main components of the used EOs were detected (Figure 1, bold colored letters). The peaks of the main EO components were rather intense, and thus, the respective calculated relative peak areas were of considerable extent (Table 1). In EO-LNPs CB, in total 10 particular peaks were found beside the regular lignin pyrolysis products detected for pure LNPs (LNPs solo) and identified as components of cinnamon bark EO. However, the two peaks 12 (cinnamic acid) and 15 (2-methoxycinnamaldehyde) were considered to be formed during pyrolysis, since the two substances were not listed in the GC profile of EO from CB (Table 6). In the case of EO-LNPs CT, beside the main peak thymol (B), also carvacrol (C), borneol (I), linalool (H), caryophyllene (G), *p*-cymene (D), and *γ*-terpinene (E) were detected. In the case of EO-LNPs WT, additionally to the main peak carvacrol, also thymol, linalool, caryophyllene, *p*-cymene, and *γ*-terpinene were found.

As mentioned above, after preparation by dialysis, aliquots of the different EO-LNP dispersions were freeze-dried and subsequently analyzed by Py-GCMS. The presence of EO components in the pyrograms of freeze-dried EO-LNPs indicated substantial association of certain components of the EOs with lignin during preparation as well as substantial retention of the volatile oils by their LNP carriers during freeze-drying, since unbound EOs were expected to get removed during freeze-drying. However, EOs attached on the surface of the LNPs could not be distinguished from EOs incorporated into the LNP molecular structure by the used Py-GCMS method. The question regarding the specific way of

DOI: 10.1021/acsomega.9b02793
ACS Omega 2020, 5, 358−368

Table 1. Relative Abundances of Pyrolysis Products from Lignin Nanoparticles Loaded with Essential Oils from Cinnamon Bark (EO-LNPs CB), Common Thyme (EO-LNPs CT), and Wild Thyme (EO-LNPs WT) As Well as Unloaded LNPs (LNPs Solo)

#	pyrolysis product	RT (min)	EO-LNPs CB (%)	EO-LNPs CT (%)	EO-LNPs WT (%)	LNPs solo (%)
D	*p*-cymene	13.23	0.1	1.2	0.3	
E	γ-terpinene	13.78		0.2	0.1	
H	linalool	18.32	0.7	1.8	0.6	
1	guaiacol	19.59	2.4	1.5	1.6	5.8
I	borneol	21.48		1.2		
2	4-methylguaiacol	23.32	0.5	0.3	0.5	0.8
A′	cinnamaldeyde (cis)	24.56	0.6			
3	4-ethylguaiacol	26.25	0.2	0.1	0.2	0.3
G	caryophyllene	27.22	9.5	0.7	0.1	
A	cinnamaldehyde (trans)	27.51	22.2			
4	4-vinylguaiacol	28.24	2.1	0.8	0.6	4.8
B	thymol	28.41		55.6	4.1	
C	carvacrol	29.15		4.4	64.6	
5/F	eugenol	29.29	5.6	0.3		0.3
6	syringol	30.14	7.3	4.7	5.3	13.8
7	isoeugenol (cis)	30.82	0.2	0.2	0.2	0.4
J	cinnamyl acetete (cis)	31.61	2.3			
8	isoeugenol (trans)	32.51	1.1	0.7	1.0	2.8
9	4-methylsyringol	33.02	1.2	0.9	1.3	1.8
10	vanillin	33.22	0.7	0.5	0.5	1.3
11	homovanillin	35.11	0.3	0.2	0.2	0.8
12	cinnamic acid	35.19	0.5			
13	4-ethylsyringol	35.27		0.3	0.4	1.0
14	acetoguaiacone	35.72	0.5	0.3	0.5	1.1
15	2-methoxycinnamaldehyde	36.20	0.8			
16	4-vinylsyringol	37.07	4.2	2.7	2.8	11.1
17	guaiacylacetone	37.34	0.5	0.3	0.3	1.3
18	4-allylsyringol	37.55	0.8	0.4	0.6	1.6
19	4-propenylsyringol (cis)	39.01	0.4	0.2	0.3	1.0
20	4-propenylsyringol (trans)	40.76	2.6	1.6	2.0	6.5
K	benzyl benzoate	41.29	4.4			
21	syringaldehyde	41.63	2.6	1.9	1.7	5.9
22	homosyringaldehyde	42.87	0.6	0.5	0.3	2.0
23	acetosyringone	43.47	1.4	1.0	0.9	2.9
24	coniferyl alcohol (trans)	44.06	5.1	4.9	2.2	13.9
25	coniferaldehyde	44.47	1.1	0.8	0.7	1.5
26	syringylacetone	44.68	1.1	0.7	0.6	2.2
27	sinapylalcohol (cis)	48.52	0.6	0.6	0.3	1.8
28	sinapylalcohol (trans)	50.86	1.6	2.2	0.5	8.6
29	sinapaldehyde	51.07	1.9	1.3	0.7	2.4

interaction between EOs and lignin molecules, for example, external adhesion or entrapment via internal incorporation, was further investigated by in vitro release studies using EO-LNP dispersions as well as redispersed freeze-dried EO-LNPs and confronting their release profiles with those obtained for pure EO aqueous dispersions.

Qualitative Analysis of Loaded EO-LNPs by FTIR Spectroscopy. FTIR spectra of freeze-dried EO-LNPs showed significant differences compared to the respective control sample of unloaded LNPs. Comparison with FTIR spectra of the respective pure EOs revealed overlapping bands (double arrows and green wavenumbers in Figure 2). Considering the workup process of freeze-drying where unbound EOs are expected to get removed, as mentioned above, the overlapping bands could indicate an intimate association between EOs and LNPs. In the case of EO-LNPs CB, two strong bands at 1720 and 1680 cm^{-1} were noted, which were attributed to the carbonyl C═O bond in cinnamaldehyde, the main component of EO from CB (Table 6). Other bands in the FTIR spectrum of pure EO-CB manifested as shoulder peaks in the spectrum of EO-LNPs CB at 1622, 1505, and 1463 cm^{-1}, which were assigned to additional aromatic skeleton vibrations, C═O stretching modes, and aromatic C−H stretching modes, respectively, deriving from cinnamaldehyde (Table 2). The increase, relative to LNPs solo, of the band at 1368 cm^{-1} in the spectrum of EO-LNPs CB could be attributed to additional phenolic hydroxyl groups deriving from eugenol as well as aliphatic C−H stretching in terminal methyl groups in eugenol, linalool, and caryophyllene. Additional G ring breathing from eugenol and again C═O stretching modes from cinnamaldehyde were considered to cause the respective increase of the bands at 1267 cm^{-1} as well as 1021 cm^{-1}. The band at 971 cm^{-1} was

DOI: 10.1021/acsomega.9b02793
ACS Omega 2020, 5, 358−368

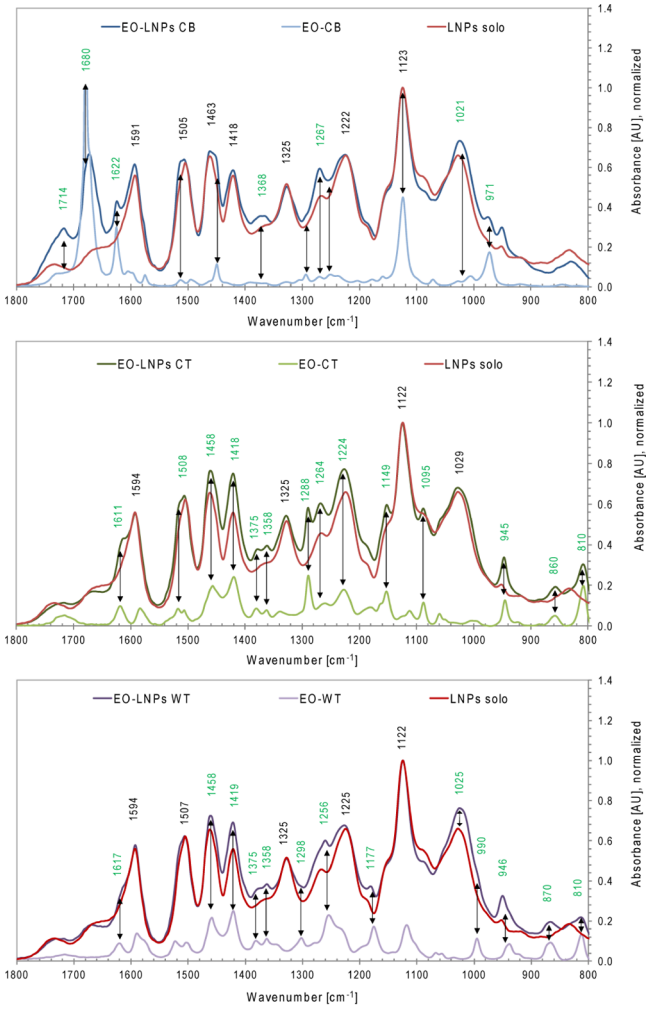

Figure 2. FTIR spectra of lignin nanoparticles loaded with the respective essential oils from cinnamon bark, common thyme, and wild thyme (EO-LNPs CB, EO-LNPs CT, and EO-LNPs WT) compared to the unloaded LNPs (LNPs solo) and the respective pure essential oils (EO-CB, EO-CT, and EO-WT).

attributed to C═C out-of-plane deformation modes deriving from double bonds in cinnamaldehyde or linalool.

In the case of EO-CT and EO-WT, which contain as main components phenolic aromatics like thymol and carvacrol, the alkylbenzene *p*-cymene, and the monoterpenes γ-terpinene and linalool, all of them with different molecular structures than common lignin monomers, several new bands beside the known lignin bands were registered. Thus, shoulders of the bands at 1611 and 1508 cm^{-1} as well as increased absorbances at 1458 and 1418 cm^{-1} were attributed to additional aromatic skeletal vibrations deriving from thymol and *p*-cymene in EO-CT. The two new bands at 1375 and 1358 cm^{-1} were assigned to terminal methyl groups in the isopropyl group in thymol, carvacrol, *p*-cymene, and γ-terpinene (Figure 7). The bands at 1288, 1264, and 1224 cm^{-1}, a spectral area representing G and S ring breathing in lignin, as well as the new bands at 1149 and 1095 cm^{-1}, in the area of aromatic C−H in-plane deformation modes, were attributed to thymol based on confrontation with a pure thymol ATR-FTIR spectrum.[24] Correspondingly, the band at 810 cm^{-1} was assigned to thymol and carvacrol as well as *p*-cymene, as they represent maxima in their respective pure

Table 2. Absorption Band Assignment in the FTIR Spectra of the Analyzed Lignin Nanoparticles Fractions[24,25a]

wavenumber (cm^{-1})	signal assignment	EO components contributions
1714	C═O stretching in aldehydes	A
1680	C═O stretching in conjugated aldehydes	A
1622−1591	aromatic skeletal vibrations, C═O stretching	A, B, C
1508−1505	aromatic skeletal vibrations	A, B, D
1463−1458	C−H deformations, asymmetric in $-CH_3$ and $-CH_2-$	A, B, C, D
1419−1418	aromatic skeletal vibrations, C−H in-plane deformation	A, B, C. D
1375−1358	aliphatic C-H stretch in $-CH_3$, not in $-OCH_3$, phenolic OH	B, C, D, E, F, G, H
1325	S plus G ring condensed ring breathing	
1298−1256	G ring breathing, C═O stretching	A, B, C, F
1225−1222	S, G ring breathing, C═O stretching	B
1177−1095	aromatic C−H in-plane deformation	B, C
1029−1021	aromatic C−H in-plane deformation, C−O stretching	A, F
990	1:2:4-substitution in carvacrol	C
971	C═C out-of-plane deformation	A, H
945	aromatic C−H out-of-plane deformation	B, C, D
870−810	aromatic C−H stretching out-of-plane S and G rings	B, C, D

[a]The one letter code in the column for the contributions of the essential oil (EO) components refers to the compounds depicted in Figure 7.

substances' FTIR spectra attributed to aromatic C−H out-of-plane deformation modes.

The FTIR spectrum of EO-LNPs WT displayed a similar situation as observed for EO-LNPs CT with some differences in the area of lignin G and S ring breathing (1300−1200 cm^{-1}). Further, a new band at 1177 cm^{-1}, located in the area of aromatic ring breathing modes and deriving from carvacrol as supported by comparison with a pure carvacrol FTIR spectrum, and an additional weak shoulder band at 990 cm^{-1}, attributed to the 1:2:4 substitution of the aromatic ring in carvacrol by Valderrama and De Gante (Figure 2), were observed.[24]

DLS Analysis of Lignin Nanoparticles Loaded with Essential Oil. The different EO-LNP dispersions were analyzed by DLS after preparation by dialysis. Average hydrodynamic diameters and polidispersity indexes (PDIs) obtained by cumulant analysis are reported in Table 3.

Table 3. Average Hydrodynamic Diameter (2*R*) and Polydispersity Indexes (PDI) Obtained by DLS Measurements of Lignin Nanoparticles (LNPs) Loaded with Essential Oils from Cinnamon Bark (EO-LNPs CB), Common Thyme (EO-LNPs CT), and Wild Thyme (EO-LNPs WT) As Well as Unloaded LNPs (LNPs Solo)[a]

sample	2*R* (nm)	PDI
LNPs solo	108.1 ± 0.4	0.048 ± 0.005
EO-LNPs CB	346.0 ± 5.0	0.140 ± 0.005
EO-LNPs CT	244.0 ± 3.0	0.110 ± 0.020
EO-LNPs WT	369.0 ± 3.0	0.140 ± 0.020

[a]Errors correspond to the standard deviation of three measurements.

DOI: 10.1021/acsomega.9b02793
ACS Omega 2020, 5, 358−368

Intensity-weighted size distributions obtained by CONTIN algorithm are shown in Figure 3. Cumulant analysis leads to an average diameter of 108 nm and a very low PDI for unloaded LNPs, confirming results of previous investigations.[26] The addition of the different EOs promoted a significant increase of the average particle size and PDI of the resulting EO-LNP fractions, which was attributed to the inclusion of the EO molecules into the LNP structure. All three EO-LNP dispersions showed a monodisperse size distribution with an average particle size varying with the used EO (Figure 3). No presence of aggregates detected in the EO-LNP dispersions.

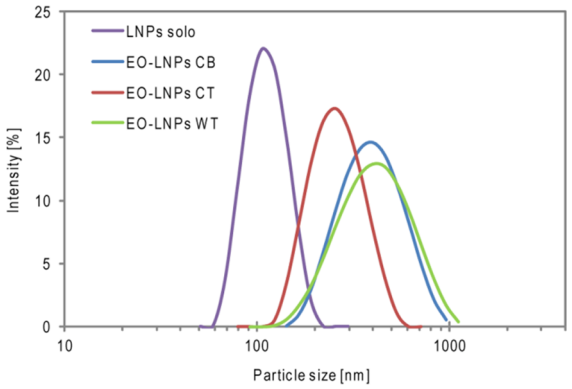

Figure 3. Intensity-weighted size distributions of lignin nanoparticles (LNPs) loaded with essential oils from cinnamon bark (EO-LNPs CB), common thyme (EO-LNPs CT), and wild thyme (EO-LNPs WT) and unloaded LNPs dispersions (LNPs solo).

SEM Analysis of Lignin Nanoparticles Loaded with Essential Oil. Particle surfaces of EO-LNPs analyzed by SEM generally showed less details and their surface appeared smoother than observed for unloaded pure LNPs in our earlier work.[26] A much higher contrast between the particle center and shell was noted, resulting in a "coated"-like appearance of EO-LNPs CB (Figure 4a,b). This effect was attributed to interactions between LNPs and essential oil molecules either superficially associated or properly incorporated into the shell of the LNPs. During the SEM experiments on EO-LNP dispersions, it was observed that EOs tended to heat up when taking up energy under the SEM electron beam with the

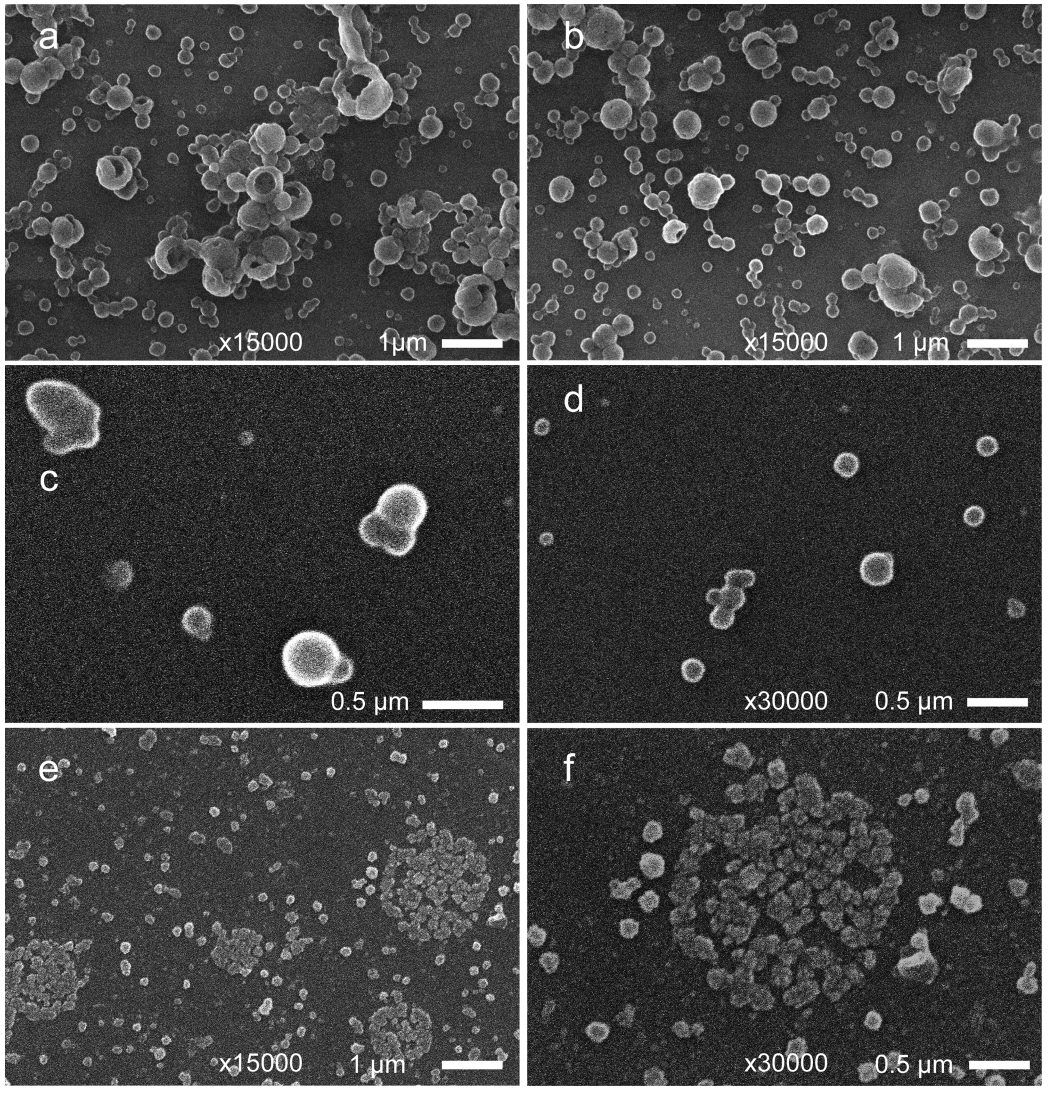

Figure 4. SEM images of (a, b) lignin nanoparticles loaded with essential oil from cinnamon bark (EO-LNPs CB dispersion), (c, d) common thyme (EO-LNPs CT dispersion), and (e, f) wild thyme (EO-LNPs WT freeze-dried).

DOI: 10.1021/acsomega.9b02793
ACS Omega 2020, 5, 358−368

consequence of a brighter appearance of the charged sample components. Therefore, the bright halo of the EO-LNPs in Figure 4 was attributed to EO molecules associated with the LNP shell. Rather, big clusters of agglomerated EO-LNPs CB in the dimension of several micrometers were identified in the SEM micrographs (Figure 4a). In a different observation, zone chain-like structures of single EO-LNPs CB with an average chain length of 4−6 single nanoparticles were spotted (Figure 4b). EO molecules, only superficially associated to the LNPs, were suspected to cause this agglomeration phenomenon observed for EO-LNPs CB. In Figure 4c,d, less concentrated zones of the EO-LNPs CT sample are displayed. EO-LNP$_S$ CT were of smaller size and less agglomeration was observed compared to EO-LNPs CB. However, the same optical effect as with EO-LNPs CB regarding their contrast between the particle center and intensely bright particle shell was imminent. In Figure 4e,f, redispersed freeze-dried EO-LNPs WT, as they were used for in vitro release studies (Figure 5b, right), are

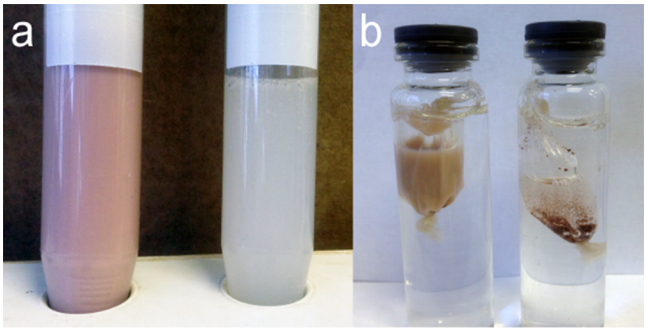

Figure 5. (a) Original dispersion of essential oil (EO)-loaded lignin nanoparticles (EO-LNPs) on the left and the respective control sample of an oil-in-water dispersion of pure EO. (b) Experimental setup for the in vitro release studies: On the left, an original EO-LNPs dispersion vs freeze-dried EO-LNPS dispersed in water (right) inside dialysis bags in the dialysis-receiving headspace glass vials.

shown. Since the freeze-dried powders were only gently dispersed in water, to avoid imminent release of the entrapped EOs through strong vortexing or sonication, agglomerates of small EO-LNPs were observed beside single EO-LNPs. The shape of freeze-dried EO-LNPs apparently changed compared to EO-LNPs observed in the respective dispersions, what might have occurred during the freeze-drying procedure.

Quantification of the Loaded EOs by RP-HPLC and in Vitro Release Studies of Loaded EOs from LNP Carriers. Figure 5a shows the fresh dispersions prepared by dialysis, starting from a solution of lignin and EO (left) as well as the control sample of a pure EO dispersion prepared the same way (right). Lignin and EO contents, determined by RP-HPLC and calculated values for their drug loading efficiencies (DLE) and drug loading capacities (DLC), are given in Table 4. In the case of CT and WT, the loaded amount of EOs in the respective LNP dispersions was considered more than efficient regarding their antimicrobial activity, because much lower concentrations in the range of 90−150 ppm were reported for the respective IC_{50} values of thymol and carvacrol against three different white-rot fungi much lower concentrations in the range of 90−150 ppm.[13] Similarly, a recent review about EOs as antimicrobial agents cited various works that found bactericidal concentration of EO-CB below the loadings of the EO-LNPs CB prepared in this work.[27]

Table 4. Lignin and Essential Oil Contents of the Different Essential Oil (EO) Containing Lignin Nanoparticle (EO-LNPs) Dispersions (disp) of Cinnamon Bark (CB), Common Thyme (CT), and Wild Thyme (WT) as well as Calculated Drug Loading Efficiencies (DLE), Drug Loading Capacities (DLC), and Yields of EO-LNPs and their Freeze-Dried Aliquots (F.D.)

EO-LNPs	lignin (mg/ml)	essential oil (mg/ml)	DLE (%)	DLC (%)	yield (%)
EO-LNPs CB disp	15.0	4.7	35.5	29.6	45.7
EO-LNPs CT disp	14.0	9.1	70.0	60.2	53.7
EO-LNPs WT disp	14.3	7.7	60.7	43.9	51.5
EO-LNPs CB F.D.			5.4	4.3	
EO-LNPs CT F.D.			38.3	32.9	
EO-LNPs WT F.D.			44.6	32.3	

Based on values for DLE and DLC, the essential oil from CB was eventually considered as the least suitable one of the tested EOs. The missing phenolic hydroxyl group of its main component cinnamaldehyde compared to lignin monomeric units might have limited EO-CB's compatibility to interact with aromatic rings of lignin units via π-stacking. The DLE values calculated for the respective EO-LNP dispersions from CT and WT instead were between 60 and 70% and thus in accordance with results presented by Dai et al. for a corresponding ratio of lignin to active ingredient of 2:1, while DLC values on the other hand were higher.[28] However, the question regarding the way of interaction between EOs and LNPs, that is, superficial association versus real entrapment via structural incorporation, needed to be investigated further since superficially attached EO molecules were not expected to show the same release behavior as properly entrapped EO molecules or free not entrapped EO micelles.

Thus, in vitro release studies were conducted with the original fresh EO-LNP dispersions as well as with freeze-dried aliquots redispersed in water (Figure 5b). Under the used experimental conditions, where turbulences by magnetic stirring inside the dialysis-receiving container were created, pure EOs dispersed in water were released very fast. Already around 80%, cumulative release (CR) was reached within the first 2 h of experiment for EO-CT and EO-WT (Figure 6 and Table 5). The release profiles of EO-LNP dispersions in the very first phase of the experiment resulted like the ones of pure EOs. However, later, the shape of the curves changed toward the form of the release profiles observed for freeze-dried EO-LNPs. This observation gave rise to the hypothesis that the EO-LNPs CB dispersion, beside EO-LNPs, also contained not entrapped pure EO micelles, forming parallel during the preparation of EO-LNPs, which leached very fast in the start of the experiment. Thus, CR after 24 h arrived at values close to the ones of pure EOs while freeze-dried EO-LNPs instead showed significantly different release profiles for both cases, CT and WT. In the first 2 h, CR remained <35% and was still lower after 24 h than after 2 h for pure EOs, indicating substantial interaction between lignin and EO molecules in the freeze-dried samples. Only after around 48 h, CR from EO-LNPs in both cases, CT and WT, surpassed 90% while the pure oils were almost completely released. Instead, for freeze-

DOI: 10.1021/acsomega.9b02793
ACS Omega 2020, 5, 358−368

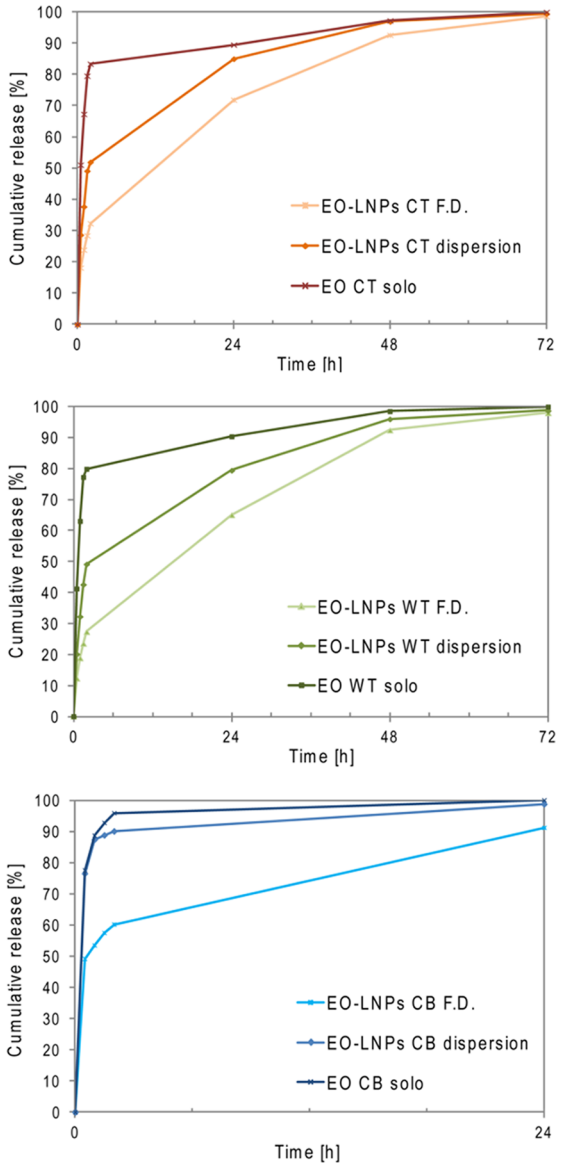

Figure 6. Release profiles of the essential oils from common thyme, wild thyme, and cinnamon bark incorporated into lignin nanoparticles (EO-LNPs CT, EO-LNPs WT, and EO-LNPs CB), used as original dispersions as well as freeze-dried (F.D.) powders, compared to the release profile of the pure EOs dispersed in water (EO-CT solo, EO-WT solo, and EO-CB solo) under identical dialysis conditions.

dried EO-LNPs from CT and WT, almost complete release was reached after 72 h of experiment (Table 5). In contrast, the release profiles of EO-LNPs CB revealed much faster leaching of EO. The time scale in the respective diagram in Figure 6 was therefore reduced to 48 h, the time point where 100% of EO from freeze-dried EO-LNPs CB was released. Complete CR for pure EO-CB was reached already after 24 h, when also 95% was released from the respective EO-LNPs CB dispersion. At this point, slightly more than 90% of EO-CB was released from freeze-dried EO-LNPs CB. Thus, molecular interaction between the main component of EO-CB cinnamaldehyde and LNPs was assumed to be rather superficial, and therefore, EO-CB was considered less suited as an active component in EO-LNPs since its retention by LNPs was the lowest among the investigated EOs, confirming the observations made above regarding DLE and DLC values (Table 4). Nevertheless, EO-LNPs CB significantly retarded the release of EO-CB into the surrounding medium compared to a pure oil-in-water emulsion as illustrated in Figure 5. Further, comparing the release profile with pure EO-CB, it was concluded that relatively more EO micelles were formed parallel to EO-LNPs CB during the dialysis process and subsequently contained in the respective EO-LNPs CB dispersion. On the other side, the main components of EO-CT and EO-WT, thymol and carvacrol, respectively, were apparently entrapped to a higher extent inside the LNP structure and less pure EO micelles were formed parallel during dialysis (Figure 6). In fact, when DLE and DLC values were also calculated for freeze-dried EO-LNPs, it was evident that the respective values presented in Table 5 for the EO-LNP dispersions needed a correction regarding the not entrapped EO. Since the difference between DLE for the EO-LNPs WT dispersion and the respective freeze-dried aliquot was the smallest, it was concluded that EO entrapment worked best for WT. While DLE for EO-LNPs CT F.D. was still acceptable, DLE for the respective sample from CB was the lowest and the earlier stipulated hypothesis regarding incompatibility of cinnamaldehyde for entrapment in LNPs was further supported. Instead, the phenolic structure of thymol and carvacrol was considered an important factor for their compatibility with lignin enabling a higher extent of molecular interaction with lignin polyphenolic structural elements via π-stacking, a process that was widely reported to be the driving force for the formation of LNPs.[28−32]

The BDSs prepared in the actual work, characterized by a strongly delayed release of the entrapped biocides, present a promising way to reduce the amounts of EOs used for biocontrol applications and thus increasing their cost-effectiveness. Through the use of wood-processing side streams for lignin isolation and preparation of nontoxic and biodegradable LNPs, costs of future products can additionally be reduced as well as environmental impacts of otherwise for energy generation used residual biomass from wood

Table 5. Cumulative Release of Essential Oil (EO) from Common Thyme (CT), Wild Thyme (WT), and Cinnamon Bark (CB) from the Respective Freeze-Dried (F.D.) EO-Loaded Lignin Nanoparticles (EO-LNPs), the Respective Original EO-LNP Dispersions (Disp.), and the Respective Control Samples of Pure EOs Dispersed in Water (EO Solo)

	essential oil cumulative release (%)								
	EO-LNPs CT			EO-LNPs WT			EO-LNPs CB		
time (h)	F.D.	Disp.	EO-CT solo	F.D.	Disp.	EO-WT solo	F.D.	Disp.	EO-CB solo
2	32.3	52.0	83.4	27.4	49.2	79.9	60.2	90.0	95.9
24	71.9	85.0	89.5	65.1	79.4	90.4	91.2	94.8	100.0
48	92.6	97.0	97.3	92.4	96.0	98.5	100.0	100.0	100.0
72	98.6	99.5	100.0	98.0	98.7	100.0			

DOI: 10.1021/acsomega.9b02793
ACS Omega 2020, 5, 358−368

Table 6. Main Components of the Used Pure Essential Oils from Cinnamon Bark (EO-CB), Common Thyme (EO-CT), and Wild Thyme (EO-WT)

EO-CB	%	EO-CT	%	EO-WT	%
t-cinnamaldehyde	69.8	thymol	47.6	carvacrol	68.5
caryophyllene	5.6	*p*-cymene	17.7	linalool	8.2
linalool	3.6	γ-terpinene	9.9	*p*-cymene	5.2
eugenol	3.1	linalool	4.7	γ-terpinene	4.0
cinnamyl acetate	2.0	carvacrol	2.8	thymol	2.6
p-cymene	1.5	caryophyllene	2.3	caryophyllene	0.9
benzyl benzoate	1.4	borneol	1.8		

processing.[33−35] The availability of considerable amounts of residual biomass offers chances for innovations and the implementation of new value chains in the wood sector, especially in areas where sawmills suffer from economic pressure to generate revenue using side and waste streams.[36−38]

CONCLUSIONS

Essential oils from cinnamon bark, common thyme, and wild thyme were successfully entrapped into lignin nanoparticles for the preparation of a bio-based biocide delivery system. Molecular interactions of essential oil compounds with lignin nanoparticles were strongly indicated based on Py-GCMS and FTIR spectroscopy. Release profiles of the essential oils from common thyme and wild thyme entrapped in lignin nanoparticles revealed significantly delayed leaching of the essential oils from the carrier material caused by substantial molecular interaction between the two partners. Essential oil from cinnamon bark instead, with the main component cinnamaldehyde, resulted less compatible for entrapment in lignin nanoparticles. The presented results will serve as a solid base for the development of a promising new green biocide delivery system based on lignin and essential oils, for example, the preservation of wood products or foodstuffs.

EXPERIMENTAL SECTION

Materials and Chemicals. Beech wood sawdust (*Fagus sylvatica* L.) from the Cimini Mountains in the Lazio region, Italy, (Piangoli Legno SNC, Soriano nel Cimino, VT, Italy) was air-dried and then cut to 35 mesh in an IKA MF 10.1 cutting mill (IKA-Werke GmbH & Co. KG, Staufen, Germany). Milled wood was then Soxhlet-extracted using acetone for 15 h and eventually dried at room temperature. 1,4-Dioxane (Alfa Aesar, ACS grade 99 + %) was purchased from Thermo Fisher (Kandel, GmbH, Karlsruhe, Germany). ACS-grade sodium hydroxide and dimethyl sulfoxide (DMSO) (>99.9%) were purchased from Carlo Erba Reagents (Milan, Italy) and Sigma-Aldrich (Milan, Italy), respectively. Pure essential oils (EOs) from cinnamon bark (*Cinnamomum zeylanicum* Blume), common thyme (*Thymus vulgaris* L.), and wild thyme (*Thymus serpyllum* L.) were purchased from FLORA Srl, Lorenzana, Italy. The main components of the pure EOs were determined by the producer FLORA Srl, using a PerkinElmer Clarus 500 GC-FID-MS system, and their respective contents and structures are given in Table 6 and Figure 7, respectively.

Lignin Extraction and Preparation of Lignin Nanoparticles (LNPs) Loaded with Essential Oils (EOs). Acidolysis lignin (AL) from beech wood sawdust was isolated as described elsewhere.[26] Lignin nanoparticles with entrapped essential oils (EO-LNPs) were prepared based on the

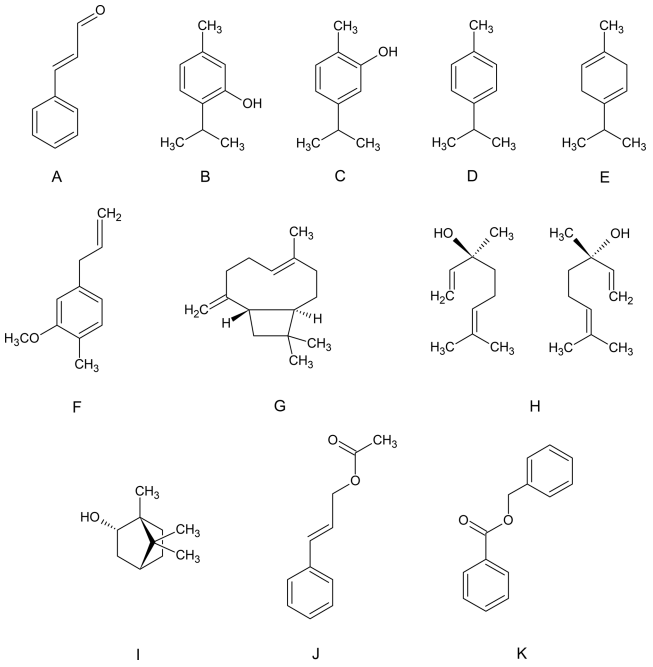

Figure 7. Structures of the main components of the respective essential oils from cinnamon bark, common thyme, and wild thyme: (A) cinnamaldehyde, (B) thymol, (C) carvacrol, (D) *p*-cymene, (E) γ-terpinene, (F) eugenol, (G) caryophyllene, (H) linalool, (I) borneol, (J) cinnamyl acetate, and (K) benzyl benzoate.

protocols presented in Zikeli et al.[23,26] with the following adaptations: After dissolving 300 mg of AL in 10 mL of DMSO, 150 μL of the respective pure EOs was added and further mixed for 5 min. After filtering through 0.45 μm CHROMAFIL Xtra syringe filters (Macherey-Nagel GmbH & Co. KG, Düren, Germany), the solutions were filled in dialysis bags (SpectraPor 1 Dialysis Membrane Standard RC Tubing, 6−8 kDa, Spectrum Labs, USA) and dialyzed against 4 L of distilled water for 1 h. A short dialysis time was chosen to prevent a concomitant release of already entrapped EOs and thus study the very first phase of EO-LNP formation. The resulting EO-LNP dispersions were stored in the fridge until further analysis. Aliquots of the EO-LNP dispersions were freeze-dried for further analysis as well as for in vitro release experiments.

Analytical Methods. *FTIR Spectroscopy.* FTIR spectra of the isolated AL fractions and the prepared LNPs as well as EO-LNPs (after freeze-drying of the dispersions) were recorded on a Jasco FTIR-4100 Fourier transform infrared spectrometer (Jasco Corporation, MD, USA). After very fine grinding of the samples in an agate mortar, potassium bromide (KBr) discs were prepared with a lignin concentration of 2 wt % using a

DOI: 10.1021/acsomega.9b02793
ACS Omega 2020, 5, 358−368

Specac Mini-Pellets Press (Specac Inc., Fort Washington, USA). The spectra were acquired in absorbance mode in the range of 4000−400 cm^{-1} with a resolution of 4 cm^{-1} against a background of pure KBr. FTIR spectra of LNPs and EO-LNPs were baseline corrected and normalized to an absorbance of 1 AU for the maximum at wavenumber 1122 cm^{-1}. Spectra of the pure EOs were normalized correspondingly at their respective maxima and then scaled for illustrative reasons in Figure 2.

Analytical Pyrolysis. Pellets from fine powdered freeze-dried EO-LNPs and pure LNPs (1.5−2 mg) were pressed in a special syringe and eventually directly pyrolyzed at 450 °C in a Pyrojector II (SGE, Inc., USA) microfurnace pyrolysis chamber. Pyrolysis products were separated in an HP 5890 Series II Plus gas chromatograph (Hewlett-Packard, DE, USA) equipped with a Restek Rtx-1701 (30 m × 0.25 mm i.d.) capillary column (Restek Corporation, PA, USA). Helium was used as carrier gas at a pressure of 100 kPa in the pyrolyzer and 70 kPa in the GC injector (280 °C, 1:20 split ratio). Oven temperature was held initially at 45 °C for 4 min and then increased to 240 °C with a heating rate of 4 °C/min and finally at a rate of 39 °C/min until 280 °C. A HP 5971A-MSD mass spectrometer was used in EI mode at 70 eV, and scans from m/z 35 to m/z 500 were run in 0.7 s cycles. Pyrolysis products were identified by mass spectra interpretation and comparison with NIST and Wiley computer libraries and the reference literature.[39−42] For each pyrogram, normalized at the most intense peak, the relative peak areas of 29 principal phenolic lignin pyrolysis products as well as the respective essential oil components were determined.

Dynamic Light Scattering (DLS). Size and size distribution of the LNP and EO-LNP suspensions were obtained by dynamic light scattering (DLS). Measurements were carried out on a Zetasizer NanoZS instrument (Malvern Instruments, U.K.) at 25 °C using the noninvasive back scattering (NIBS) technique with a detection angle of 173°, which is less sensitive to multiple scattering effects compared to the more conventional 90° geometry.[43] The measured DLS autocorrelation functions were analyzed using the cumulant method to obtain the average hydrodynamic diameter of the particles and the polydispersity index (PDI)[44] and by CONTIN algorithm to obtain the size distribution.[45] Results are presented as an average of three measurements per sample with the respective standard deviations.

Reversed Phase HPLC: Essential Oil Loading and in Vitro Release Studies. LNPs and EO-LNPs were analyzed using a Varian 2510 HPLC system with a Varian 2550 variable wavelength detector using acetonitrile−water as a mobile phase (70:30 mixture (v/v), 0.7 mL/min flow, detection at 280 nm) and a EC NUCLEODUR C18 Isis (5 μm particle size, 4.6 mm × 150 mm) reversed phase HPLC column (Macherey-Nagel GmbH & Co. KG, Düren, Germany). External calibration for quantification was done with dilutions of the used pure essential oils. EO-LNP dispersions were injected after dilution in the mobile phase, and freeze-dried samples were dissolved in the mobile phase in the concentration of 1 mg/mL before injection. Drug loading efficiency (DLE) and drug loading capacity (DLC) were calculated according to the following equations as published elsewhere:[28]

$$\text{DLE (\%)} = (\text{weight of EO in EO} - \text{LNPs} / \text{weight of EO added initially}) \times 100 \quad (1)$$

$$\text{DLC (wt\%)} = (\text{weight of EO in EO} - \text{LNPs} / \text{weight of EO} - \text{LNPs}) \times 100 \quad (2)$$

Release of EOs from the respective LNPs was investigated by a dialysis method, based on the method published by Dai et al.[28] EO-LNP dispersions as well as control samples of the respective pure EO dispersions were filled into a dialysis bag, which was immersed into 18 mL of distilled water inside a 20 mL headspace vial, closed with a rubber stopper, and sealed with Parafilm. Freeze-dried EO-LNPs (15 mg/mL) were added to 0.9 mL of distilled water, gently redispersed, and filled inside a dialysis bag, which was successively used as described above (Figure 5b). Samples from the dialysis-receiving container were taken with a Hamilton 100 μL glass syringe through the rubber stopper and directly injected into the HPLC system to avoid evaporation of essential oil. Water in the dialysis-receiving container was changed every 24 h and sampling was conducted in 0.5 h time intervals within the first 2 h of experiment, successively in 24 h periods.

Scanning Electron Microscopy (SEM). For preparation of the samples for SEM, drops of the EO-LNP suspensions as well as drops of redispersed freeze-dried EO-LNPs were adsorbed onto a glass coverslip and air dried at 25 °C. The cover slips were in turn attached to aluminum stubs using carbon tape and sputter-coated with gold in a Balzers MED 010 unit (Oerlikon Balzers, Balzers, Liechtenstein). SEM analysis was conducted with a JSM 6010LA electron microscope (JEOL Ltd., Tokyo, Japan).

AUTHOR INFORMATION

Corresponding Authors

*E-mail: zikeli@unitus.it (F.Z.).
*E-mail: gscaras@unitus.it (G.S.M.).
*E-mail: mroma@unitus.it (M.R.).

ORCID

Simona Sennato: 0000-0003-4793-5359
Giuseppe Scarascia Mugnozza: 0000-0003-0357-4360

Notes

The authors declare no competing financial interest.

ACKNOWLEDGMENTS

The work was conducted in the frame of the PRIN-MIUR 2015 (Research Projects of National Interest by the Italian Ministry of Education, University and Research) "Wood value-chain" project (grant no.: 2015YW8JWA, coordinator: G.S.M.). Further support was received by the "Departments of Excellence-2018" program (Dipartimenti di Eccelenza) of the Italian Ministry of Education, University and Research for the project "Landscape 4.0 − food, wellbeing and environment" of the Department for Innovation in Biological, Agro-Food and Forest Systems (DIBAF) of the University of Tuscia. The authors gratefully acknowledge the support with SEM experiments from Anna Rita Taddei, Interdepartmental Centre of Electron Microscopy CIME, University of Tuscia.

REFERENCES

(1) Moscatelli, M.; Romagnoli, M.; Cenfi, S.; Lagomarsino, A.; Di Tizio, A.; Spina, S.; Grego, S. Wood-soil interactions in soil bioengineering slope stabilization works. *iFOREST* **2009**, *2*, 187−191.
(2) European Commitee for Standardization. *EN 335:2013: Durability of wood and wood-based products − Use classes: definitions,*

DOI: 10.1021/acsomega.9b02793
ACS Omega 2020, 5, 358−368

application to solid wood and wood-based products; BSI Standards Limited: Brussels, Belgium, 2013.
(3) Blanchette, R. A.; Nilsson, T.; Daniel, G.; Abad, A. Biological Degradation of Wood. In *Archaeological Wood*; American Chemical Society: Washington, DC, 1989; Vol. *225*, pp 141−174, DOI: 10.1021/ba-1990-0225.ch006.
(4) Wong, A. H. H.; Check, K. S. *Observations of Termite-fungus Interactions of Potential Significance to Wood Biodeterioration and Protection*. Timber Technology Centre *Bulletin*: Kuala Lumpur, Malaysia, 2001, *24*, 1−8.
(5) De Angelis, M.; Romagnoli, M.; Vek, V.; Poljanšek, I.; Oven, P.; Thaler, N.; Lesar, B.; Kržišnik, D.; Humar, M. Chemical composition and resistance of Italian stone pine (Pinus pinea L.) wood against fungal decay and wetting. *Ind. Crops Prod.* **2018**, *117*, 187−196.
(6) Romagnoli, M.; Segoloni, E.; Luna, M.; Margaritelli, A.; Gatti, M.; Santamaria, U.; Vinciguerra, V. Wood colour in Lapacho (Tabebuia serratifolia): chemical composition and industrial implications. *Wood Sci. Technol.* **2013**, *47*, 701−716.
(7) Romagnoli, M.; Fragiacomo, M.; Brunori, A.; Follesa, M.; Scarascia Mugnozza, G. Solid Wood and Wood Based Composites: The Challenge of Sustainability Looking for a Short and Smart Supply Chain. In *Digital Wood Design: Innovative Techniques of Representation in Architectural Design*; Bianconi, F.; Filippucci, M. Eds. Springer International Publishing: Cham, Switzerland, 2019; pp 783−807.
(8) Romagnoli, M.; Vinciguerra, V.; Silvestri, A. Heat Treatment Effect on Lignin and Carbohydrates in Corsican Pine Earlywood and Latewood Studied by PY−GC−MS Technique. *J. Wood Chem. Technol.* **2018**, *38*, 57−70.
(9) Romagnoli, M.; Cavalli, D.; Pernarella, R.; Zanuttini, R.; Togni, M. Physical and mechanical characteristics of poor-quality wood after heat treatment. *iFOREST* **2015**, *8*, 884−891.
(10) Madrid, F.; Rubio-Bellido, M.; Villaverde, J.; Peña, A.; Morillo, E. Natural and assisted dissipation of polycyclic aromatic hydrocarbons in a long-term co-contaminated soil with creosote and potentially toxic elements. *Sci. Total Environ.* **2019**, *660*, 705−714.
(11) Jones, A. S.; Marini, J.; Solo-Gabriele, H. M.; Robey, N. M.; Townsend, T. G. Arsenic, copper, and chromium from treated wood products in the U.S. disposal sector. *Waste Manage.* **2019**, *87*, 731−740.
(12) Duncan, D. L.; Carls, M. G.; Rice, S. D.; Stekoll, M. S. The toxicity of creosote-treated wood to Pacific herring embryos and characterization of polycyclic aromatic hydrocarbons near creosoted pilings in Juneau, Alaska. *Environ. Toxicol. Chem.* **2017**, *36*, 1261−1269.
(13) Zhang, Z.; Yang, T.; Mi, N.; Wang, Y.; Li, G.; Wang, L.; Xie, Y. Antifungal activity of monoterpenes against wood white-rot fungi. *Int. Biodeterior. Biodegrad.* **2016**, *106*, 157−160.
(14) Ben Arfa, A.; Combes, S.; Preziosi-Belloy, L.; Gontard, N.; Chalier, P. Antimicrobial activity of carvacrol related to its chemical structure. *Lett. Appl. Microbiol.* **2006**, *43*, 149−154.
(15) Sadiki, M.; El Abed, S.; Balouiri, M.; Barkai, H.; El Bergadi, F. Z.; El Farricha, O.; Ibnsouda Koraichi, S. Combined effect of essential oils against bacteria associated with deterioration of historical wood. *J. Mater. Environ. Sci.* **2017**, *8*, 594−602.
(16) Salem, M. Z. M.; Zidan, Y. E.; Mansour, M. M. A.; El Hadidi, N. M. N.; Abo Elgat, W. A. A. Antifungal activities of two essential oils used in the treatment of three commercial woods deteriorated by five common mold fungi. *Int. Biodeterior. Biodegrad.* **2016**, *106*, 88−96.
(17) Singh, T.; Singh, A. P. A review on natural products as wood protectant. *Wood Sci. Technol.* **2012**, *46*, 851−870.
(18) Borges, C. C.; Tonoli, G. H. D.; Cruz, T. M.; Duarte, P. J.; Junqueira, T. A. Nanoparticles-based wood preservatives: the next generation of wood protection? 2018, *24* (4), 397−407, DOI: 10.1590/01047760201824042531.
(19) Mattos, B. D.; Tardy, B. L.; Magalhães, W. L. E.; Rojas, O. J. Controlled release for crop and wood protection: Recent progress toward sustainable and safe nanostructured biocidal systems. *J. Controlled Release* **2017**, *262*, 139−150.
(20) Vinciguerra, V.; Spina, S.; Luna, M.; Petrucci, G.; Romagnoli, M. Structural analysis of lignin in chestnut wood by pyrolysis-gas chromatography/mass spectrometry. *J. Anal. Appl. Pyrolysis* **2011**, *92*, 273−279.
(21) Figueiredo, P.; Lintinen, K.; Hirvonen, J. T.; Kostiainen, M. A.; Santos, H. A. Properties and chemical modifications of lignin: Towards lignin-based nanomaterials for biomedical applications. *Prog. Mater. Sci.* **2018**, *93*, 233−269.
(22) Sipponen, M. H.; Lange, H.; Crestini, C.; Henn, A.; Österberg, M. Lignin for Nano- and Microscaled Carrier Systems: Applications, Trends, and Challenges. *ChemSusChem* **2019**, *12*, 2039−2054.
(23) Zikeli, F.; Vinciguerra, V.; D'Annibale, A.; Capitani, D.; Romagnoli, M.; Scarascia Mugnozza, G. Preparation of Lignin Nanoparticles from Wood Waste for Wood Surface Treatment. *Nanomaterials* **2019**, *9*, 281.
(24) Valderrama, A. C. S.; De, G. C. R. Traceability of Active Compounds of Essential Oils in Antimicrobial Food Packaging Using a Chemometric Method by ATR-FTIR. *Am. J. Anal. Chem.* **2017**, *08*, 726−741.
(25) Faix, O. Fourier Transform Infrared Spectroscopy. In *Methods in Lignin Chemistry*; Lin, S. Y.; Dence, C. W., Eds.; Springer Berlin Heidelberg: Berlin, Heidelberg, 1992; pp 233−241, DOI: 10.1007/978-3-642-74065-7_16.
(26) Zikeli, F.; Vinciguerra, V.; Taddei, A. R.; D'Annibale, A.; Romagnoli, M.; Mugnozza, G. S. Isolation and characterization of lignin from beech wood and chestnut sawdust for the preparation of lignin nanoparticles (LNPs) from wood industry side-streams. *Holzforschung* **2018**, *72*, 961−972.
(27) Wińska, K.; Mączka, W.; Łyczko, J.; Grabarczyk, M.; Czubaszek, A.; Szumny, A. Essential Oils as Antimicrobial Agents—Myth or Real Alternative? *Molecules* **2019**, *24*, 2130.
(28) Dai, L.; Liu, R.; Hu, L.-Q.; Zou, Z.-F.; Si, C.-L. Lignin Nanoparticle as a Novel Green Carrier for the Efficient Delivery of Resveratrol. *ACS Sustainable Chem. Eng.* **2017**, *5*, 8241−8249.
(29) Zhou, Y.; Han, Y.; Li, G.; Chu, F. Effects of Lignin-Based Hollow Nanoparticle Structure on the Loading and Release Behavior of Doxorubicin. *Materials* **2019**, *12*, 1694.
(30) Zhou, Y.; Han, Y.; Li, G.; Yang, S.; Xiong, F.; Chu, F. Preparation of Targeted Lignin−Based Hollow Nanoparticles for the Delivery of Doxorubicin. *Nanomaterials* **2019**, *9*, 188.
(31) Frangville, C.; Rutkevičius, M.; Richter, A. P.; Velev, O. D.; Stoyanov, S. D.; Paunov, V. N. Fabrication of environmentally biodegradable lignin nanoparticles. *ChemPhysChem* **2012**, *13*, 4235−4243.
(32) Qian, Y.; Deng, Y.; Qiu, X.; Li, H.; Yang, D. Formation of uniform colloidal spheres from lignin, a renewable resource recovered from pulping spent liquor. *Green Chem.* **2014**, *16*, 2156−2163.
(33) Pieratti, E.; Paletto, A.; Atena, A.; Bernardi, S.; Palm, M.; Patzelt, D.; Romagnoli, M.; Teston, F.; Grega, V. E.; Grebenc, T.; Krajnc, N.; Schnabel, T. Environmental and climate change impacts of eighteen biomass-based plants in the alpine region: A comparative analysis. *J. Cleaner Prod.* **2020**, *242*, 118449.
(34) Paletto, A.; Bernardi, S.; Pieratti, E.; Teston, F.; Romagnoli, M. Assessment of environmental impact of biomass power plants to increase the social acceptance of renewable energy technologies. *Heliyon* **2019**, *5*, No. e02070.
(35) Vinardell, M. P.; Mitjans, M. Lignins and Their Derivatives with Beneficial Effects on Human Health. *Int. J. Mol. Sci.* **2017**, *18*, 1219.
(36) Delfanti, L. M. P.; Bedini, R.; Romagnoli, M.; Recanatesi, F.; Meacci, F.; Caruso, L.; Manzo, A.; Salvati, L. Estimation of agroforestry biomasses available for energy purposes in a municipality in central Italy as instrument for energy planning. *Appl. Math. Sci.* **2014**, *8*, 6577−6587.
(37) Colantoni, A.; Recanatesi, F.; Baldini, S.; Felicetti, M.; Romagnoli, M. Decision analysis for the determination of biomass in the territory Tuscia Romana by geographic information system and forest management plans. *J. Agric. Eng.* **2013**, *44*, e4.
(38) Zambon, I.; Monarca, D.; Cecchini, M.; Bedini, R.; Longo, L.; Romagnoli, M.; Marucci, A. Alternative energy and the development

DOI: 10.1021/acsomega.9b02793
ACS Omega 2020, 5, 358−368

of local rural contexts: an approach to improve the degree of smart cities in the Central-Southern Italy. *Contemp. Eng. Sci.* **2016**, *9*, 1371−1386.
(39) Faix, O.; Meier, D.; Fortmann, I. Thermal degradation products of wood: Gas chromatographic separation and mass spectrometric characterization of monomeric lignin derived products. *Holz Roh-Werkst.* **1990**, *48*, 281−285.
(40) Faix, O.; Meier, D.; Fortmann, I. Thermal degradation products of wood: A collection of electron-impact (EI) mass spectra of monomeric lignin derived products. *Holz Roh- Werkst.* **1990**, *48*, 351−354.
(41) Faix, O.; Fortmann, I.; Bremer, J.; Meier, D. Thermal degradation products of wood: Gas chromatographic separation and mass spectrometric characterization of polysaccharide derived products. *Holz Roh- Werkst.* **1991**, *49*, 213−219.
(42) Faix, O.; Fortmann, I.; Bremer, J.; Meier, D. Thermal degradation products of wood: A collection of electron-impact (EI) mass spectra of polysaccharide derived products. *Holz Roh- Werkst.* **1991**, *49*, 299−304.
(43) Kaszuba, M.; Connah, M. T. Protein and Nanoparticle Characterisation Using Light Scattering Techniques. *Part. Part. Syst. Charact.* **2006**, *23*, 193−196.
(44) Koppel, D. E. Analysis of Macromolecular Polydispersity in Intensity Correlation Spectroscopy: The Method of Cumulants. *J. Chem. Phys.* **1972**, *57*, 4814−4820.
(45) Provencher, S. W. A constrained regularization method for inverting data represented by linear algebraic or integral equations. *Comput. Phys. Commun.* **1982**, *27*, 213−227.

DOI: 10.1021/acsomega.9b02793
ACS Omega 2020, 5, 358−368